Computational Aesthetics in Graphics, Visualization, and Imaging (2008)
P. Brown, D. W. Cunningham, V. Interrante, and J. McCormack (Editors)

Applications of High Precision Imaging Polarimetry

L. Neumann[1], R. Hegedus[2], G. Horvath[2] & R. Garcia[3]

[1]Computer Vision and Robotics Group, University of Girona, and ICREA, Spain.
[2]Biooptics Laboratory, Department of Biological Physics, Eötvös University, Budapest, Hungary.
[3]Computer Vision and Robotics Group, University of Girona, Spain.

Abstract

We propose the use of imaging polarimetry for general photography, which is a relatively young technique allowing the determination of polarized components of the light coming from extended objects or scenes. In this paper high resolution and accurate methods are introduced to determine the two linearly polarized components (Q,U) of light.
The CIE Luv color space is used in this work to visualize the triplet of (I,Q,U) polarization image components. The structure of this color space is also highly appropriate to represent other attributes of linearly polarized light, such as the polarized intensity, degree and the angle of polarization.
The accurately measured polarization components can also be efficiently used for image enhancement. In this direction, a new, polarization-based de-reflection method is proposed. This method is an optimal pixel-wise extension of the widely used photographical polarization filtering. Our method is also capable of amplifying the specular effects. Another application is de-hazing, which removes the linearly polarized component of the haze present in natural scenes, and results in a sharp and color-corrected image. Furthermore, the different combinations of visible and infrared polarization channels enable great possibilities in further de-hazing and to create artistic images.

Categories and Subject Descriptors (according to ACM CCS): I.3.3 [Computer Graphics]: Picture/Image Generation

1. Introduction

Human vision is practically "polarization-blind" [HV04]. We can distinguish a wide range of colors in our rich light environment, while it is impossible for us to see differences between lights with the same spectral, but different polarization characteristics. Perception of light polarization, however, is widely exploited in animal vision [Koe85, HV04]. We can be aware of the effects of linear polarization only in an indirect way, by using linearly polarizing filters and observing the scenes across differently oriented filter positions. This method is well known in photography due to its interesting and practical possibilities. By rotating a linearly polarizing filter in front of the camera lens, we can see the changes in intensity and color of the sky, plants or the water surface, for instance. Thus, we can ensure a maximal dynamic range and saturation of the sky, as well as an enhanced contrast and intense colors for the plants in a sunny landscape. Rayleigh scattering causes the polarization of sky-light. Furthermore, light also becomes polarized when it is reflected or refracted. Examples of such polarization effects can be observed in the image reflected by a window. In this case, an appropriately rotated linear polarization filter can be used to see a clear image appearing behind the glass (thus, removing the reflection). In photography, an optimal direction has to be selected for the transmission axis of the polarizing filter at the time of acquiring the image, and this orientation applies for all the pixels of the image.

Using imaging polarimetry [HV04] it is possible to measure the full polarization information at pixel-resolution. In the case of linear polarization two polarization component images are formed in addition to the light intensity component for every color channel. Therefore, we have 3 images for every (r,g,b) color channel. The 3×3 images contain all polarization information (except for the circularly polarized light component, which is not considered in this paper, but will be briefly described in Section 2). We have a wide range

© The Eurographics Association 2008.

delivered by EUROGRAPHICS DIGITAL LIBRARY www.eg.org diglib.eg.org

of possible image manipulations having the 3×3 images, and they can be visualized in many different ways. Thereby, 9 values are available for every pixel, and these 9 values can be combined in triplets to represent *rgb*-pixel values. A given combination can be just a mathematical function resulting in an artistic effect, but could also have a direct physical meaning. For instance, unwanted specular reflections can only be removed in standard photography by using a globally optimal orientation of the linearly polarizing filter. Imaging polarimetry opens new doors to optimizing such effects locally at the pixel level.

The paper is organized as follows. Sections 2 and 3 describe the physical background and mathematical model of polarized light. Section 4 introduces an automated calibration of the Mueller matrix of the polarizing filter mounted on the camera, having a central importance in the model using a non-convex optimization. Then, section 5 demonstrates the application of CIE Luv color space for visualization of the linear polarization channels. Some interesting and useful applications are illustrated in section 6, such as the enhancement or elimination of specular reflections. Another application is de-hazing, which ensures color restoration and sharpness of scenes blurred by haze without knowing the distance of objects (depth values), scattering or absorption parameters, and the sun position. Finally, we present an example of imaging polarimetry performed in the near infrared domain, which is really beyond the sensibility of the human eye.

2. Polarization of light

Polarization is a characteristic property of transverse waves, which oscillate in a plane that is perpendicular to their direction of propagation. Since light is a transverse electromagnetic wave, composed of a coupled electric and magnetic field, polarization is one of its basic feature beyond intensity and wavelength. From the fundamental laws of electrodynamics it follows that there is no general restriction how the plane of oscillation of the electric field (and of the magnetic field as well, which we do not consider further, as its plane of oscillation is always perpendicular to that of the electric field, thus sharing the same polarization properties) is oriented apart from it being perpendicular to the direction of propagation, i.e, this plane can be arbitrary. In reality, when a light beam consists of waves vibrating in all the possible planes with a uniform distribution and intensity, that light is unpolarized. In contrast, when in a light beam only waves with one distinct oscillation plane are present, that light is said to be totally linearly polarized. Another mode of polarization can be figured when during the propagation of light the end-point of the electric field vector traces out a circle in a selected plane perpendicular to the direction of propagation. In this case, depending on the handedness of the rotation of the electric field vector, that can be counter-clockwise or clockwise, the light is left or right circularly polarized, respectively. Generally, a light beam is elliptically polarized, which is developed by the superposition of a linear and a circular component. Furthermore, a part of the beam can be unpolarized, in this case it is called partially polarized light.

In the nature a beam of light from any object that reaches our eye or a light detector is most probably partially linearly polarized due to the fact that in certain frequently occurring interactions with media, like reflection, refraction and scattering, a light beam becomes more or less linearly polarized [Koe85, HV04]. These phenomena ascertain that the light from our world is diversely polarized and, in addition to radiance and color, polarization becomes another dimension among the properties of light, which can hold precious information about the media from which the light is reflected, or in which it is scattered, for example. In nature these information are indeed utilized by a lot of animals, which are capable of perceiving light polarization [Koe85, HV04].

The polarizational state of a light beam at a given wavelength can be described by four independent parameters. In this paper we apply the Stokes formalism, according which a vector with four components $\underline{S} = (S_0, S_1, S_2, S_3)^\mathsf{T} = (I, Q, U, V)^\mathsf{T}$, the so-called Stokes-vector is assigned to the light beam. Component I is the total intensity of light, while Q and U describe linear polarization and V circular polarization. The basis of this representation is that a light wave can be always resolved into two arbitrarily chosen orthogonal components: for linear polarization the phase shift between these components is equal to 0 or π, but the amplitude of the two component can be different, thus two parameters are required for the description of linearly polarized light. On the other hand, for circular polarization the phase shift is $\pi/2$ or $3\pi/2$ (for left and right circular polarization, respectively), and the amplitudes of the two components are the same, i.e. one additional parameter describes circular polarization.

Correspondingly, to any medium or optical element a 4×4 matrix (the so-called Mueller-matrix) can be assigned, which describes how the given medium at a given spatial arrangement makes changes to the polarizational state of light with it getting in a certain interaction, like refraction, reflection, transmission or scattering [Col93]. Thus the $\underline{S}'$ polarizational state of the light after the interaction can be easily determined by the matrix operation: $\underline{S}' = \underline{\underline{M}} \cdot \underline{S}$, where $\underline{\underline{M}}$ is the Mueller-matrix of the medium and$\underline{S}$ is the Stokes-vector describing the polarizational state of the incident light before the interaction.

In our paper we are only dealing with linear polarization, therefore we apply Stokes-vectors reduced to their first three components and reduced 3×3 Mueller-matrices of optical elements, which only affect linear polarization.

There are certain physical quantities that can be derived from the Stokes-vector components, which provide us with illustrative information about the linear polarization state of a light beam, and which are also used in this work:

$$I_{POL} = \sqrt{Q^2 + U^2} \tag{1}$$

© The Eurographics Association 2008.

is the polarized intensity, i.e. the intensity of the polarized part of the light, which is less than or equal to I. In the special case when $I_{POL} = I$, the light is totally linearly polarized. Furthermore,

$$p = \frac{\sqrt{Q^2+U^2}}{I} = \frac{I_{POL}}{I} \tag{2}$$

is called the degree of linear polarization, which ranges between 0 and 1, and describes how strongly the light beam is linearly polarized. $\chi = \frac{1}{2} tan^{-1}\left(\frac{U}{Q}\right)$ is the angle of polarization that gives the orientation of the plane, in which the electric field of the linearly polarized part of the light beam is oscillating.

3. Determining the linear polarizational state of light

In order to be able to determine the polarizational state of a light beam, first we need to keep in mind that in a direct way we are only able to measure intensity, i.e. the first Stokes-vector component by using a light detector, be it photoreceptors in an eye, or a CCD/CMOS sensor in a camera. This means that the linear polarizational state of light can only be determined by performing at least three independent measurements, in which the same light goes through an analyzer that differently makes change in the intensity of light depending on its linear polarization throughout the measurements. The most straightforward optical element to be applied as linear polarization analyzer in such measurements is a linear polarizer, the characteristic property of which is that it attenuates unequally the orthogonal components of an optical beam transmitted through it. An ideal linear polarizer only transmits the component, the electric field of which oscillates in the plane parallel to the transmission axis of the polarizer, while the component perpendicular to it is completely attenuated. Thus the linear polarizer produces a totally linearly polarized light from any light getting through it. More important for us, however, is that the intensity of light transmitted through the polarizer depends on the linear polarization of the incident light and as well as on the orientation of the transmission axis of the polarizer. In a left-handed three-dimensional coordinate system, in which xy is the oscillatory plane and axis z is the line of propagation of the light, the Mueller-matrix of an ideal linear polarizer that has a transmission axis parallel to axis x [Col93]:

$$\underline{\underline{M}}_{LIN}(\theta = 0^\circ) = \frac{1}{2}\begin{pmatrix} 1 & 1 & 0 \\ 1 & 1 & 0 \\ 0 & 0 & 0 \end{pmatrix}, \tag{3}$$

where θ is measured counterclockwise from the horizontal axis x.

The Mueller-matrix $\underline{\underline{M}}$ of an optical element at a given spatial arrangement, after having been rotated counterclockwise by θ around axis z, is transformed into $\underline{\underline{M}}(\theta)$ as follows:

$$\underline{\underline{M}}(\theta) = \underline{\underline{M}}_{ROT}(-\theta) \cdot \underline{\underline{M}} \cdot \underline{\underline{M}}_{ROT}(\theta) \tag{4}$$

where

$$\underline{\underline{M}}_{ROT}(\theta) = \begin{pmatrix} 1 & 0 & 0 \\ 0 & \cos 2\theta & \sin 2\theta \\ 0 & -\sin 2\theta & \cos 2\theta \end{pmatrix} \tag{5}$$

is the Mueller-matrix of the rotator, i.e. an operator that rotates the orthogonal components of a light beam equally by an angle θ.

Thus, the Mueller matrix of an ideal linear polarizer with its transmission axis set at an angle measured counterclockwise from axis x:

$$\underline{\underline{M}}_{LIN}(\theta) = \frac{1}{2}\begin{pmatrix} 1 & \cos 2\theta & \sin 2\theta \\ \cos 2\theta & \cos^2 2\theta & \sin 2\theta \cos 2\theta \\ \sin 2\theta & \sin 2\theta \cos 2\theta & \sin^2 2\theta \end{pmatrix} \tag{6}$$

Let the original linear polarizational state of the investigated light beam be

$$\underline{S}_o = \begin{pmatrix} I \\ Q \\ U \end{pmatrix}, \tag{7}$$

which is transmitted through a linear polarizer. Then the measured intensity $I_M(\theta)$ of transmitted light depending on the orientation of the transmission axis of the polarizer is going to be the first component of the resultant vector from the operation $\underline{\underline{M}}_{LIN}(\theta) \cdot \underline{S}_o$:

$$I_M(\theta) = \left(\underline{\underline{M}}_{LIN}(\theta) \cdot \underline{S}_o\right)_0 = \frac{1}{2}\left(I + Q\cos 2\theta + U \sin 2\theta\right) \tag{8}$$

From this formula it clearly follows that by measuring the intensity of light transmitted through the linear polarizer at three different orientations of its transmission axis we end up with a linear equation system, from which the (I,Q,U) values can be unambiguously obtained. This is the standard method of measuring linear polarization.

4. Imaging polarimetry and a new method of evaluation

4.1. Pixel-wise polarization information

The above method can be used not only for measuring the state of linear polarization of a homogenous light beam, but, since a linear polarizing filter retains the image of any object seen through it, it allows for simultaneously determining the polarizational state of light coming from several points of the given object. This kind of measurement is called imaging polarimetry, which is a decent and robust method for acquiring spatially detailed information about the polarization characteristics of an object or a scene. Since its pioneering development in the 1980's, imaging polarimetry has been systematically applied for in-depth studies of polarization patterns of skylight [GHMRW01, HBG*02] and freshwater surfaces [HV97], for example, which are crucial in the orientation of numerous animals capable of perceiving linear polarization. In effect, an imaging polarimeter is a camera

© The Eurographics Association 2008.

with a linear polarizer mounted on it in front of its lens. A measurement is performed by shooting the same scene with at least three different orientation θ_i $(i = 1 \ldots K, K \geq 3)$ of the transmission axis of the polarizer. This way for every pixel j $(j = 1...N)$ and in every color channel c (that can usually be red, green and blue on standard cameras) a spectrally averaged $I^{(c)}_{M[j]}(\theta_i)$ intensity is acquired. Considering each pixel independently and applying the above method of evaluation, we can obtain a Stokes-vector for every pixel j and color channel c:

$$\underline{S}^{(c)}_j = \begin{pmatrix} I^{(c)}_j \\ Q^{(c)}_j \\ U^{(c)}_j \end{pmatrix} \tag{9}$$

Note that since $I^{(c)}_j$ is the original intensity of pixel j in color channel c, by performing these operations, beyond pixelwise acquisition of the linear polarization characteristics of the acquired scene also its original image is restored, i.e. how it should look without applying a linear polarizer. Hence we also call it naked-eye intensity. A crucial point of the evaluation is that the angles θ_i of the transmission axis of the polarizer measured from a reference direction must be known and be reproducible within a sufficient precision. Usually it is ascertained by a precalibration process of the experimental setup, which can produce angle settings with a precision around 1 degree. An obstacle of reaching a higher precision is the error of reproduction of the angle settings during a measurement. In a usual setup where the linear polarizer is rotated by hand during a polarimetric measurement it takes several seconds to acquire a complete image sequence required for the evaluation. Any shaking of the camera, moving of the photographed object or scene or change in the environmental illumination results in awkward artifacts in the calculated polarization patterns. Thus except for laboratory lighting conditions and still objects, it is preferable to shoot the image sequence as fast as possible, while a more precise setting and reproduction of θ_i angles certainly would slow down the image capturing process.

We present below a novel refinement of the above evaluation technique, elaborated for reaching higher precision in acquisition of polarization data in ordinary imaging polarimetry. Let us assume that the θ_i angles are known and define for a given pixel j and color channel c a quadratic regression error $H^{(c)}_j$ as:

$$H^{(c)}_j = \sum_{i=1}^{K} \left[I^{(c)}_{M[j]}(\theta_i) - \frac{1}{2}\left(I^{(c)}_j + Q^{(c)}_j \cos 2\theta_i + U^{(c)}_j \sin 2\theta_i \right) \right]^2 \tag{10}$$

where $I^{(c)}_{M[j]}(\theta_i)$ are the known measured intensities of pixel j at color channel c and at the angle of the transmission axis of the polarizer θ_i for every i. K is the number of different alignments of the polarizer through which the images are taken. We have to select $K > 3$ to ensure a "freedom factor" for the regression. By searching for $\min\left[H^{(c)}_j\right]$, the conditions $\frac{\partial H^{(c)}_j}{\partial I^{(c)}_j} = 0$, $\frac{\partial H^{(c)}_j}{\partial Q^{(c)}_j} = 0$ and $\frac{\partial H^{(c)}_j}{\partial U^{(c)}_j} = 0$ yield a linear equation system, from which the values of $I^{(c)}_j$, $Q^{(c)}_j$ and $U^{(c)}_j$ are obtained. After the Stokes-vectors

$$\underline{S}^{(c)}_j = \begin{pmatrix} I^{(c)}_j \\ Q^{(c)}_j \\ U^{(c)}_j \end{pmatrix}$$

for each pixel j at every color channel c have been calculated, a total regression error H can be given by

$$H = \sum_{j=1}^{N} \sum_{c} H^{(c)}_j \tag{11}$$

where $H^{(c)}_j$ is obtained by substituting the previously determined $I^{(c)}_j$, $Q^{(c)}_j$, $U^{(c)}_j$ values.

4.2. Automated Parameter Calibration Process

The equations 10 and 11 provide the idea of a two-pass automatic parameter calibration. In the first pass we can determine the θ_i values as well as the real exposure times, which will differ from their nominal values. The total regression error of a well selected sample pixel set will be minimal in the case of the exact θ_i and exposure values. The first pass is practically a non-convex optimization of $2K-1 = 17$ unknowns (with K being the number of filter orientations). In the second pass, once the angles and exposures have been obtained from the first pass, we can compute the regression for all the pixels to determine the unknown (I,Q,U) image triplets for the three color channels. In order to apply method described above, we have built an imaging polarimeter composed of a Canon EOS 40D DSLR camera, with a B+W F-PRO Käsemann linear polarizer mounted in front of a Canon EF 1.4/35mm L USM lens. We have selected nine different settings for the orientation of transmission axis of the polarizer, separated from each other by approximately the same angle (about 20 degrees). For every polarimetric measurement, nine images of the same scene are taken. Later, these images are used for the evaluation of the polarimetric data. The images are acquired with the same optical and exposure settings of the camera, and stored as raw images retaining 14-bit precision of radiance per color channel (red, green, blue). The actual orientations of the polarizer have an unknown error, being different from their nominal values θ^{NOM}_i. Furthermore, the actual exposure times (which differs from the nominal value due to the mechanical shutter) often deviates up to $20-30\%$ from their preset value.

For each exposure i we consider an f_i multiplicative correction factor. The factor f_1 can be arbitrarily set to 1. The evaluation is then started by selecting appropriate pixels for the calculation of the regression error. To ensure a high accuracy, we take the raw images and select pixels from the

© The Eurographics Association 2008.

middle zone of their dynamic range, avoiding over and underexposed values. The number of pixel samples N_s can be significantly smaller than the total number of pixels. In our case, we selected N_s between 3,000 and 10,000. Minimizing the regression error (see eq. 13) for this subset of pixels, the real angle and exposure values are obtained. The error for pixel j can be expressed as:

$$H_j^{(c)}\left(\{\theta_i, f_i\}_{i=1..K}\right) = \sum_{i=1}^{K}\left[f_i I_{M[j]}^{(c)}(\theta_i) - \frac{1}{2}\left(I_j^{(c)} + Q_j^{(c)}\cos 2\theta_i + U_j^{(c)}\sin 2\theta_i\right)\right]^2 \tag{12}$$

The total regression error can be obtained by summing eq. 12 for all the selected sample pixels N_s:

$$H\left(\{\theta_i, f_i\}_{i=1..K}\right) = \sum_{j=1}^{N_S}\sum_{c} H_j^{(c)} \tag{13}$$

In this first step, eq. 13 presents a 17-variable non-convex minimization problem (the unknowns are the 9 angles + 8 exposure correction factors). Of course, mathematically, the total number of variables is $17 + 3 \cdot N_s$. However, in this first pass, we are only interested in the 17 calibration unknowns. This non-linear minimization has various additional constraints. An evident upper bound of the objective function is of the total regression error of the nominal angles and exposure times. Other constraints are prescribed for the angles and for their differences. Moreover, lower-upper bounds for the exposure times are set.

To carry out this optimization, a brute force Monte Carlo process has been applied in this paper. Some heuristics have been used to accelerate the convergence, as well as to avoid getting stuck in local minima.

To illustrate the results of the non-convex minimization, let us see the θ_i angles in Table 1. It shows the nominal and calibrated values obtained as result of the optimization applied to one of our test images.

Table 1: *(Nominal vs. Calibrated Angle).*

(0, 1.126)	(20, 24.345)	(40, 45.118)
(60, 61.441)	(80, 77.370)	(100, 95.766)
(120, 112.85)	(140, 132.43)	(160, 153.01)

The method described above ensures a new quality level of imaging polarimetry. We obtain a high-resolution and accurate polarization image set for every wavelength or color channel. Starting from 12-14 bit raw images, and computing an accurate pre-calibration based on images taken with more than 3 different orientations of the polarizer (in our case 9 different orientations), the accuracy of the polarization imaging increases significantly, ensuring new possibilities.

5. Visualization

5.1. The (I,Q,U) - CIE Luv analogy

CIE Luv is approximately a perceptually uniform color space. It uses a so called translational (Judd-type) white point adaptation [Fai98],defined by the (X_n, Y_n, Z_n) white point. We will use by default the D65 white point, but we could also use the measured values of the color temperature of the illumination of the scene. Historically CIE Luv and CIELAB were adopted simultaneously by the CIE when no clear consensus could be formed behind only one or the other of these two color spaces.

CIE Luv provides a natural analogy to the (I,Q,U) polarization image components, which will be used in order to visualize the results of imaging polarimetry in a clear and reproducible way. The intensity I corresponds to the luminance L^*, and the (Q,U) polarization components correspond to the (u^*, v^*) opponent color color channels of CIE Luv.

The formulas of CIE Luv with the standard CIE 1976 L*u*v* notation are the follows.

$$\begin{aligned}
&L^* = 116\left({}^{Y}/_{Y_n}\right)^{1/3} - 16, \quad if\ {}^{Y}/_{Y_n} > t,\ t = \left({}^{6}/_{29}\right)^3\\
&L^* = {}^{8}/_{t}\left({}^{Y}/_{Y_n}\right), if {}^{Y}/_{Y_n} \le t\\
&u^* = 13L^*\left(u' - u'_n\right) = L^* u_{rel}\\
&v^* = 13L^*\left(v' - v'_n\right) = L^* v_{rel}\\
&(L^*, u^*, v^*) = L^*(1, u_{rel}, v_{rel})
\end{aligned} \tag{14}$$

where u' and v' are determined from the CIE XYZ color coordinates [CIE86]:

$$\begin{aligned}
u' &= \frac{4X}{X+15Y+3Z}\\
v' &= \frac{9Y}{X+15Y+3Z}
\end{aligned} \tag{15}$$

u' and v' are the horizontal and vertical coordinates of Fig. 1(a).The attributes derived from (L^*, u^*, v^*) are the hue h_{uv}, chroma C^* and saturation s_{uv}:

$$\begin{aligned}
h_{uv} &= \arctan\left(\frac{v^*}{u^*}\right)\\
C^* &= \sqrt{u^{*2} + v^{*2}} = L^*\sqrt{u_{rel}^2 + v_{rel}^2}\\
s_{uv} &= \frac{C^*}{L^*} = \frac{\sqrt{u^{*2}+v^{*2}}}{L^*} = \sqrt{u_{rel}^2 + v_{rel}^2},\ if\ L^* > 0
\end{aligned} \tag{16}$$

Let us recall from imaging polarimetry the basic derived attributes. We can discover a natural analogy with the CIE Luv space: $(I,Q,U) \sim (L^*, u^*, v^*)$. Similarly, for the derived attributes:

$$I_{POL} = \sqrt{Q^2 + U^2} \sim C^* = \sqrt{u^{*2} + v^{*2}} \tag{17}$$

© The Eurographics Association 2008.

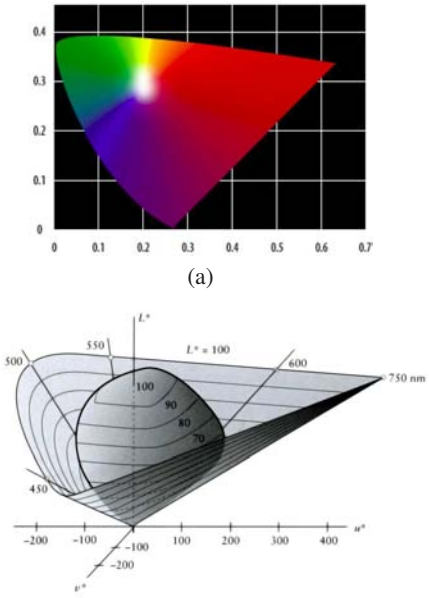

(a)

(b)

Figure 1: *(a) 2D representation of the CIE Luv space: u' denotes the horizontal axis and v' the vertical axis. (b) Shape of the theoretical Luv space and the solid color gamut in 3D. The LCD and printers have a differently shaped gamut.*

polarized intensity vs. chroma,

$$p = \frac{\sqrt{Q^2+U^2}}{I} = \frac{I_{POL}}{I} \sim s_{uv} = \frac{\sqrt{u^{*2}+v^{*2}}}{L^*} \in [0,1] \quad (18)$$

linear degree of polarization vs. saturation, and

$$2\chi = \arctan\left(\frac{U}{Q}\right) \sim h_{uv} = \arctan\left(\frac{v^*}{u^*}\right) \quad (19)$$

angle of polarization vs. hue.

5.2. Visualization using the CIE Luv analogy

Every row of Table 2 contains 3 basic and 3 derived polarization attributes of a given color channel. By selecting 3 of these attributes, we can create a new color image using the CIE Luv analogy. Consider the (I,Q,U) triplet for a given pixel and a given color channel. We can consider this triplet as the (L^*,u^*,v^*) components, and visualize it after transforming it into RGB values. In order to accomplish this, first we have to re-scale the I to the $[0,100]$ range of L^*. Then, (Q,U) have to be appropriately calibrated to prevent the color from falling outside the gamut, or if they are too small, the image would be unsaturated.

Naive compression of the minimal and maximal L-values of the 14-bit raw image would result in a boring appearance, since a reduced number of extreme dark or bright pixels cause the dominant part of the image to have a small luminance range. Therefore, the solution to this problem is to let a given percentage of pixels to fall out of the selected range, thus, being clipped. A solution to find the optimal interval is the use of the minimal information loss method [NMP98]. A similar problem appears for the (Q,U) components. It is desirable to increase their value to obtain high chroma. In LCDs or printers, the shape of the gamut is very irregular: saturated blues are dark, saturated yellows are bright, etc. We applied an interval halving method to ensure that a small percentage of pixels is clipped due to the high chroma values (see Fig. 1-b). In this case, we have taken into consideration the Luv gamut obtained from the sRGB space.

Table 2: *Basic and derived RGB-polarization attributes.*

I_R	Q_R	U_R	I^R_{POL}	p_R	χ_R
I_G	Q_G	U_G	I^G_{POL}	p_G	χ_G
I_B	Q_B	U_B	I^B_{POL}	p_B	χ_B

5.3. RGB visualization of the degree of linear polarization and polarized intensity

While in section 5.2 we selected attributes taking a row of Table 2, each of the 6 columns of the table can also be selected to visualize its components in RGB. The first column corresponds to the visible image with naked eye (i.e., RGB intensities without any filtering). The second and third column depict the Q and U polarization components of the RGB channels. The fourth column is the Pythagorean length of (Q,U), i.e., the *polarized intensity*. The last two columns are the degree and angle of linear polarization, as described in eqs. 18 and 19, respectively. In all 6 cases, we applied a similar parameter calibration to exploit the available gamut as described in section 5.2.

6. Application for Imaging

High-quality imaging polarimetry can be applied to a real photographic application for the removal (or amplification) of the polarization components of an image. Since specular reflection and scattering makes the light partly polarized, there is a possibility of efficient photographic reduction or even elimination of disturbing specular reflections. Moreover, the haze present in natural scenes can also be reduced (or removed) for distant objects. In the past there were several attempts to accomplish this task [SNN03, SN05], but none of them utilized high-precision pixel-wise polarization information. These approaches rely on a basic physical model incorporating scattered air-light and the light originating from distant objects behind the haze, where only a global degree of polarization is determined and used. In contrast, our approach exploits local polarization data, furthermore it

© The Eurographics Association 2008.

avoids any ambiguities arising from an additional physical model, since it is merely based on the measured polarization characteristics.

In order to realize the above photographic enhancements, consider the following general equation:

$$I_{DEP} = I - f(I,Q,U) \cdot I_{POL} \tag{20}$$

where I_{DEP} is the intensity of the resulting depolarized image, and $f(I,Q,U)$ corresponds to an appropriately chosen multiplicator. We remind the reader that for the I_{POL} polarized intensity the following constraint holds:

$$0 \leq I_{POL} = \sqrt{Q^2+U^2} \leq I \tag{21}$$

When $f(I,Q,U) \equiv 1$, we obtain the *exact depolarization* case, that is, removing the polarization component from the image (see Fig. 3g). This case provides an image with less specular reflections or less blurring and degradation of visibility caused by haze. However, both scattering and reflection usually yield a non-polarized component as well, which are not removed from the image in the exact depolarization case. The selection of $f(I,Q,U)$ in between 1 and 0 leads to a partial depolarization.

If $f(I,Q,U) \geq 1$, and we ensure the positivity of eq. 21, we achieve the over-depolarization range. Thus we can reduce more intensively the non-polarized components of specular reflection and haze (see Figs. 2 and 3h). However, for artistic applications we can also amplify the specular or haze effects by choosing $f(I,U,V) < 0$ (see Fig. 3f).

There are further possibilities granted by utilizing the photographic imaging polarimetry outside the visible spectral domain, i.e., in the ultraviolet or near infrared (NIR) ranges. Thereby we can obtain further artistic imaging (see Fig. 4). We can also utilize the infrared range in the de-hazing process. For instance, a natural scene is much less prone to blurring due to haze in this spectral domain, due to the λ^{-4} wavelength dependency of Rayleigh scattering.

Note that the high precision of our imaging polarimetric method is highly exploited to achieve depolarization with photographic image quality and low level of noise. We emphasize, however, that our current results are preliminary. The determination of optimal $f(I,Q,U)$ multiplicators and other contributing factors for the most effective de-reflection and de-hazing process needs further elaboration.

7. Conclusions

Imaging polarimetry has been applied in the past to scientific applications such as astronomy, microscopy, bio-optical research, or sky-cloud observation. In this paper we extended the use of imaging polarimetry to the field of general photography. This technique requires the acquisition of a sequence of images, placing a polarizing filter in front of the camera lens, and setting its transmission axis at minimally 3 different orientations. Our two-step method carries out first an auto-calibration by a non-convex optimization based on a sample pixel set to determine the real values of the orientation angles of the filter and the small differences from the nominal exposure times. Then, in the second step we compute the (I,Q,U) intensity and polarization components for all the RGB color channels by means of a pixel-wise regression.

Another contribution of this paper is the introduction of the CIE Luv space as a natural analogy to visualize imaging polarimetry in a descriptive way. This representation of imaging polarimetry ensures reproducible false coloring. That is, after adequate training, the viewer would be able to "see" the nature of the polarization components of a scene.

For every color channel, we can observe the intensity, the degree and the angle of polarization as independent images. Moreover, any given attribute, e.g. the degree of polarization, can be visualized in his "eigen-color" in the form of a unified RGB color image. The visualization of the otherwise humanly invisible polarized components produces interesting results and may have an aesthetical appearance.

On the other hand, a real application of imaging polarimetry in the field of general photography is the removal of the polarized part of the intensity. Specular reflection and Rayleigh scattering are a source of polarized light. Thereby the removal of the polarized intensity reduces or eliminates only the unwanted reflection effects, such as the haze effect that limits the visibility. Some preliminary examples of imaging-polarimetry-based depolarization and over-depolarization have been presented. We also studied the polarization at non-visible NIR wavelengths.

We are working in the exploration of the ultraviolet range, which is rich in scattering, having a special importance in animal vision. Furthermore we are also investigating the possibilities of a high quality imaging polarimetry with particular attention to circular polarization. This field is problematic and needs special care, since the relative intensity of the circular component under natural lighting conditions usually falls below 1-2% compared to the total intensity of light. Our new technique is capable of reducing the noise also here, and ensures new possibilities. In the future we will explore further applications, as well as aesthetical possibilities, by combining the image intensity, the linearly and circularly polarized components.

Acknowledgments

This work has been partially funded through the MOMARNET EU project MRTN-CT-2004-505026, in part by the FREESUBNET EU project MRTN-CT-2006-036186 and in part by the Spanish Ministry of Education and Science under grant CTM2007-64751. LN wish to thank ICREA for their

© The Eurographics Association 2008.

support. RH and GH wish to thank Alexander von Humboldt Foundation for equipment donation.

References

[CIE86] CIE: Colorimetry, second edition: Cie publication 15.2, 1986.

[Col93] COLLETT E.: *Polarized Light - Fundamentals and Applications*. Marcel Dekker, Inc., New York - Basel - Hong Kong, 1993.

[Fai98] FAIRCHILD M. D.: *Color Appearance Models*. Addison-Wesley, Reading, MA, 1998.

[GHMRW01] GAL J., HORVATH G., MEYER-ROCHOW V. B., WEHNER R.: Polarization patterns of the summer sky and its neutral points measured by full-sky imaging polarimetry in finnish lapland north of the arctic circle. *Proceedings of the Royal Society A 457* (2001), 1385–1399.

[HBG*02] HORVATH G., BARTA A., GAL J., SUHAI B., HAIMAN O.: Ground-based full-sky imaging polarimetry of rapidly changing skies and its use for polarimetric cloud detection. *Applied Optics 41*, 3 (2002), 543–559.

[HV97] HORVATH G., VARJU D.: Polarization pattern of freshwater habitats recorded by video polarimetry in red, green and blue spectral ranges and its relevance for water detection by aquatic insects. *Journal of Experimental Biology 200* (1997), 1155–1163.

[HV04] HORVATH G., VARJU D.: *Polarized Light in Animal Vision Polarization Patterns in Nature*. Springer-Verlag, Heidelberg -Berlin - New York, 2004.

[Koe85] KOENNEN G. P.: *Polarized Light in Nature*. Cambridge University Press, Cambridge, 1985.

[NMP98] NEUMANN L., MATKOVIC K., PURGATHOFER W.: Automatic exposure in computer graphics based on the minimum information loss principle. In *Proceedings of Computer Graphics International (CGI '98)* (Los Alamitos, CA, 1998), IEEE Computer Society Press, pp. 666–679.

[SN05] SCHECHNER Y., NAYAR S.: Generalized mosaicing: Polarization panorama. *IEEE Transactions on Pattern Analysis and Machine Intelligence 27*, 4 (2005), 631–636.

[SNN03] SCHECHNER Y., NARASIMHAN S., NAYAR S.: Polarization-Based Vision through Haze. *Applied Optics, Special issue 42*, 3 (Jan 2003), 511–525.

© The Eurographics Association 2008.

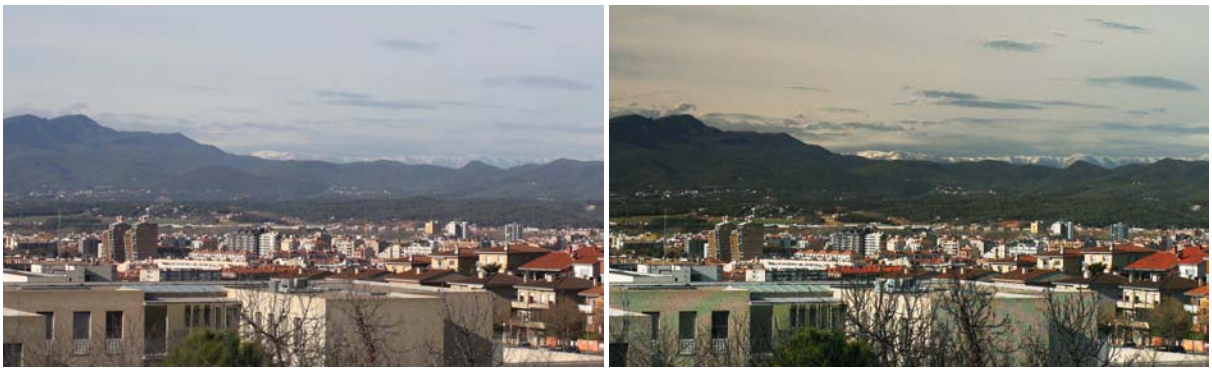

Figure 2: *Example of de-hazing in a landscape photograph. (left) Naked-eye image containing blurred and bluish far mountains. (right) Resulting image after the over de-polarization according to equation 20. Haze is highly removed, the greenish color and the sharpness of the mountains are restored. The polarized bluish color of the sky is also removed, emphasizing the clouds.*

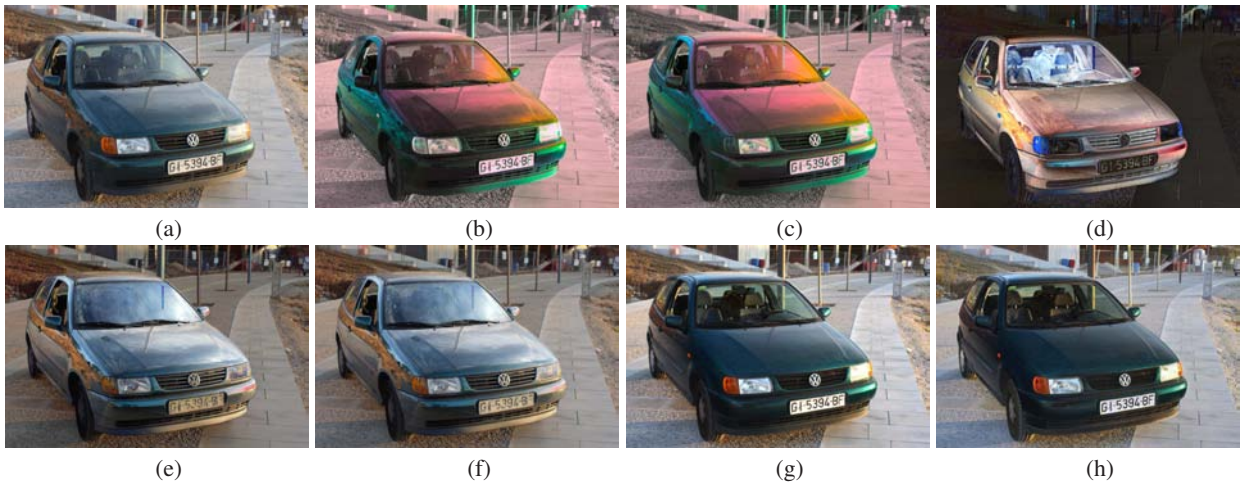

Figure 3: *(a) Naked-eye image. (b) and (c) (I,Q,U) polarized triplet visualized using CIE Luv space for the R and G channels, respectively. (d) RGB image of the degree of polarization. Greenish colors of the car and the orange lamp appear in their (approx.) complementary color. This kind of changes often occurs in imaging polarimetry. (e) Polarized intensity. (f) Emphasized reflection effects through over-polarization. (g) and (h) Exact depolarization and over-depolarization images, respectively.*

Figure 4: *Near infrared image of the University Campus. The images were acquired with an infrared-converted Canon 30D camera using a Heliopan Infrared 715 NIR filter. The colors coming from the different infrared sensitivity curves of the RGB channels of the CMOS sensor. (left) Original acquired image. (middle) Image after de-polarization. Although infrared is not so rich in scattering as the bluish wavelengths, we can still remove some haze effects in NIR. Note how the details of mountains are sharper, the sky is darker due to the removed polarized intensity. (right) Degree of polarization unified in an RGB image.*

© The Eurographics Association 2008.